Autoionization phenomena involving the $2p^5 3d$ configuration of argonlike ions in ionic solids

M. Elango, A. Ausmees, A. Kikas, E. Nõmmiste, R. Ruus, and A. Saar
Institute of Physics, Estonian Academy of Sciences, Riia 142, EE2400 Tartu, Estonia

J. F. van Acker, J. N. Andersen, and R. Nyholm
Department of Synchrotron Radiation Research, Lund University, Sölvegatan 14, S-223 62 Lund, Sweden

I. Martinson
Department of Atomic Spectroscopy, Lund University, Sölvegatan 14, S-223 62 Lund, Sweden
(Received 4 August 1992)

The photon-induced Auger and photoelectron spectra of the argonlike ions Cl^- (in NaCl), K^+ (in KCl), Ca^{2+} (in $CaCl_2$ and CaF_2), and Sc^{3+} (in Sc_2O_3) have been measured in the vicinity of the L_{23} absorption edges of these ions. It is shown that at the $2p^6 \rightarrow 2p^5 3d(4s)$ resonance a spectator structure appears in the $L_{23}M_{23}M_{23}$ Auger spectra, which shifts to higher kinetic energies with increasing photon energy. This structure originates from the $3p^{-2}3d(4s)$ final configuration arising as a product of the Auger resonant-inelastic-scattering process of the incident photons. We demonstrate that the peculiarities of this process and the role of the collapsing $3d$ electron in it can be largely understood in terms of an atomic treatment. The solid-state effects, caused by the crystal field and the lattice polarization, may play an additional role.

I. INTRODUCTION

The Auger spectra, photoexcited in the regions of inner-shell ionization threshold of atoms, molecules, and solids provide sensitive probes for the dynamics of inner-shell transitions.[1] In such an excitation the creation and the decay of the inner-shell hole cannot in principle be considered as separate processes, and interesting phenomena like resonant scattering and postcollision interaction (PCI) occur (see, e.g., a recent review[2]).

Here we present the results of a study of these phenomena in the case of resonant photoionization of the $2p^6$ shell of the argonlike ions Cl^-, K^+, Ca^{2+}, and Sc^{3+} in ionic solids. The photoabsorption may be described here as a transition $2p^6 \rightarrow 2p^5 3d(4s)$ in the particular ion, possibly modified by the crystal field. The important point is that the final configuration $3d$ shell collapses (i.e., its radial wave function suddenly contracts) in the sequence $Cl^- \rightarrow Ar \rightarrow K^+$, as shown by means of the absorption and emission studies of Ref. 3. We anticipated observing the results of this collapse in the relevant Auger spectra, and in this way obtaining new information on the effect of the presence of an excited $3d$ electron on the decay dynamics of the $2p$ hole.

It turned out that in all cases studied here the photocreation of the $2p^6 \rightarrow 2p^5 3d(4s)$ resonance gives rise to new structures in the photoemission spectrum. One conspicuous structure is situated in the region of the normal $L_{23}M_{23}M_{23}$ Auger spectrum, but differs from it in two important aspects: it is excitable only at the resonance photon energies and it shifts to higher kinetic energies when the photon energy increases in the resonance region. It follows from empirical considerations and atomic calculations that this structure originates from the $3p^{-2}3d(4s)$ final configuration. In a fully consistent picture the whole process should be described as a single Auger resonant inelastic scattering event. However, we show that to a good approximation it may be treated as a two-step process: the resonant photoexcitation followed by the $3d(4s)$ spectator-affected $L_{23}M_{23}M_{23}$ Auger decay of the $2p$ hole. We also present evidence that shake processes do not contribute to the formation of the final configuration due to the collapse of the $3d$ shell in the configuration $2p^5 3d$ of K^+, Ca^{2+}, and Sc^{3+}.

Details of the experimental procedure are presented in Sec. II. Section III deals with the theoretical background and our treatment of the two-step approach. A general interpretation of the experimental results is given in Sec. IV, while a more detailed discussion of the autoionization process and a detailed comparison with theoretical calculations in the case of KCl is given in Sec. V. We separately discuss shake probabilities in Sec. VI, and summarize our main conclusions in Sec. VII.

II. EXPERIMENTAL

The experiments were carried out using synchrotron radiation from beamline 22 at MAX-Laboratory, Lund University, Sweden.[4] The monochromator was a modified SX-700 plane-grating monochromator, with energy resolution better than 0.3 eV in the 200- to 400-eV-photon energy region. The absorption spectra were recorded by detecting the total electron yield. For the absolute calibration of the photon energy, we have taken advantage of the radiation in second order diffraction from the monochromator. At the photon energy at which the absorption edge occurs two measurements of a photoemission core level are performed, one with the use of first-order light, and one using second-order light. The difference in kinetic energy for the photoelectron peak in these two

spectra is equal to the photon energy at the absorption edge.

The samples were films of NaCl, KCl, CaF_2, $CaCl_2$, and Sc_2O_3, all but Sc_2O_3 prepared by thermal evaporation *in situ* from a molybdenum boat onto polished copper substrates in a vacuum of 5×10^{-7} Torr. The Sc_2O_3 film was prepared elsewhere by electron beam evaporation. The film thickness (about 200 Å and the evaporation rate (several Å/s) were controlled by a quartz crystal monitor. The vacuum in the experimental chamber was 2×10^{-10} Torr. No sample charging effects greater than 0.1 eV were observed in the experiments.

The electron energy spectra were recorded by means of a hemispherical electron energy analyzer (Scienta ESCA SES-200). A typical electron energy resolution was set to 0.15 eV. The binding energy scales for the different compounds are given so that zero binding energy corresponds to the bottom of the conduction band. This was achieved by measuring all photoemission binding energies with respect to the top of the valence band and then adding the band-gap energies [8.5 eV for NaCl,[5] 8.4 eV for KCl,[5] 6.9 eV for $CaCl_2$,[6] 12.1 eV for CaF_2,[7] and 6.0 eV for Sc_2O_3 (Ref. 8)] to the measured values.

III. COMPUTATIONS

In terms of a two-step approach the resonant Auger emission intensity can be given as

$$I(E,h\nu)\sim\sum_{if}A(h\nu_i-h\nu)B(E_{if}-E)\ . \tag{1}$$

Here E is the Auger energy and $h\nu$ is the photon energy; i refers to the intermediate state and f to the final state. $A(h\nu_i-h\nu)=\sigma_i L(h\nu_i-h\nu)$ is the population of the excited $2p^5 3d$ $(4s)$ configuration, σ_i is the photoexcitation cross section (from the ground state to the state i), and $L(h\nu_i-h\nu)$ is a line profile which includes the monochromator resolution, total Auger decay width and solid-state broadening.[9] $B(E_{if}-E)=W_{if}G(E_{if}-E)$ is the Auger energy distribution curve, where W_{if} is the Auger decay rate and $G(E_{if}-E)$ represents a line profile which in principle should include the experimental broadening, the Auger decay width, and also a phonon contribution.[10] In the following we have represented this line profile by a Lorentzian. For the photoionized $2p^5$ intermediate configuration of the normal Auger process we have assumed that the intermediate levels i are uniformly populated with a statistical weight of $2J_i+1$ (J_i is the total quantum number for the state i).

The Auger transition rate from the intermediate state i to the final ionic state f with continuum wave functions $|\varepsilon lj\rangle$ normalized to represent one ejected electron per unit time is for the atomic case[11]

$$W_{if}=\sum_j\left|\sum_\mu\sum_{\mu'}C_{i\mu}C_{f\mu'}\langle\gamma'L'S'J'\varepsilon ljJ|\sum_{\alpha<\beta}1/r_{\alpha\beta}|\gamma LSJ\rangle\right|^2, \tag{2}$$

where L, S, J (or L',S',J') are the orbital, spin, and total quantum numbers of the intermediate (or final ionic) state of the ion (γ and γ' includes whatever other quantum numbers are required). $C_{i\mu}$ and $C_{f\mu}$, are mixing coefficients for the states i and f in the intermediate coupling scheme. In intermediate coupling the spin-orbit interaction is treated as a perturbation which couples different states $|SLJ\rangle$ with the same J, constructed as zero-order wave functions in LS coupling. The total angular momenta J' and j of the final ionic states and the continuum electron, respectively, are recoupled in the final state of the system. The transition matrix elements in Eq. (2) can be evaluated by using the Jj-LS unitary transformation. Then

$$\left\langle\gamma'L'S'J'\varepsilon ljJ\left|\sum_{\alpha<\beta}1/r_{\alpha\beta}\right|\gamma LSJ\right\rangle=[(2L+1)(2S+1)(2j+1)(2J'+1)]^{1/2}\begin{Bmatrix}L' & l & L\\ S' & \frac{1}{2} & S\\ J' & j & J\end{Bmatrix}\left\langle\gamma'L'S'\varepsilon lLSJ\left|\sum_{\alpha<\beta}1/r_{\alpha\beta}\right|\gamma LSJ\right\rangle, \tag{3}$$

In the configuration interaction approach we used the wave functions for each state written as a linear combination of basis wave functions, each of which represents a particular single-configuration state in the LS coupling scheme. For the determination of the Auger decay of the $2p^5 3d$ excited state only the most important final configurations $3s^2 3p^4 3d$, $3s^2 3p^4 4s$, and $3s 3p^6$ are included in the configuration interaction calculations. The necessary calculations for the various atomic configurations of the ions are performed using a self-consistent-field procedure within the nonrelativistic single-electron Hartree-Fock-Pauli (HFP) approximation.[12] This approximation uses the radial wave functions of the zero-order Hartree-Fock (HF) Hamiltonian and takes into account the relativistic effects as corrections of the order α^2 (α is the fine structure constant). The matrix elements for the Coulomb and spin-orbit interaction are calculated using the HF radial wave functions and the matrix is diagonalized to yield eigenvalues and eigenvectors. The term-dependent effects in the energy level structures are expected to be small and therefore the configuration-average HF method is used. The continuum wave functions εl are generated by solving the HF equations corresponding to the final ionic states. The energy dependence and the term dependence for the continuum wave functions are found to be small and so the

averaged transition energy and the configuration-averaged coefficients of the final states are used.

The photoexcitation cross sections σ_i for the $2p^5 3d$ excited states of the argonlike ions K^+ and Ca^{2+} from the $J=0$ ground state to a state $J=1$ are computed using the dipole transition operator in the "length form." The resultant branching ratios are quite different from the statistical 2:1 ratio which indicates a quite strong deviation from the *jj*-coupling scheme. In the coupling conditions of the $2p^5 3d$ excited states the spin-orbit coupling of the $2p$ hole is the strongest interaction. The spin-orbit interaction of the collapsed $3d$ electron is weaker than its electrostatic interaction with the core hole. This points out that in the case of the $2p^5 3d$ excited states the coupling scheme is near to a *jK* coupling scheme.[11]

To obtain the electronic wave functions for the ions in the crystals we have used the HFP approximation in conjunction with the Watson sphere model.[13] In this model, the influence of the solid matrix on the electrons of an ion is simulated by superimposing on the potential of the free ion an additional potential due to a hollow sphere with charge $-Q=(Z-N)e$ and an appropriately chosen depth V_c or radius R of this potential well. Thus, the Hamiltonian in the crystal in this model is given by

$$H_{\rm cr}=H_0+\sum_{i=1}^{N} V(r)\ , \tag{4}$$

where H_0 is the Hamiltonian for a free ion with nuclear charge Ze and N electrons and

$$V(r)=\begin{cases} V_c=Qe/R & \text{for } r\le R\ , \\ Qe/r & \text{for } r>R\ . \end{cases} \tag{5}$$

We used values of V_c equal to the Madelung energies of the crystals (for KCl, for example, this is 8.00 eV and for CaF_2 19.98 eV).

When a photoelectron or an Auger electron is ejected, the medium responds by polarization, which decreases the total energy of the final state left behind by the extra-atomic relaxation energy E_p.[14] We computed the binding and Auger energies in the crystals as $E_B=E_0-E_p$ for the photoelectron binding energies, $E_A^*=E_0+E_p$ for the Auger energies of the excited (nonionized) initial states, and $E_A=E_0+3E_p$ for the Auger energies of the ionized initial states (two final hole states). Here E_0 is the difference of the total energies of initial and final states of the ions in the Watson sphere. For E_p we used the values estimated for NaCl (1.58 eV) and KCl (1.97 eV) in Ref. 15 and for CaF_2 (1.73 eV) in Ref. 16. Because the ionicity of Sc_2O_3 is considerably less than for other compounds studied here, our model is not appreciable in this case.

IV. RESULTS AND GENERAL DISCUSSION

In Figs. 1(a)–1(e) we show the total electron yield spectra for NaCl, KCl, CaF_2, $CaCl_2$, and Sc_2O_3 in the vicinity of the Cl, K, Ca, and Sc L_{23} absorption edges. They agree well with the corresponding absorption spectra[3,9,17] and have been fully explained in previous studies, on an atomic as well as on a solid-state level.[9,18,19] The main maxima of these spectra are due to transitions into states related to $2p^5(3s^2 3p^6)ns$ and $2p^5(3s^2 3p^6)nd$ configurations of the ions, the latter being strongly dominant. They are accompanied by resonant emission bands, which indicates that the arising final states are well-localized atomiclike states.[3] For KCl, CaF_2, $CaCl_2$, and Sc_2O_3 the four strongest bands correspond to the collapsed $2p^5(3s^2 3p^6)3d$ configuration in the solid state and in a first approximation they reflect the spin-orbit splitting (by about 2.7 eV for K, 3.4 eV for Ca, and 4.5 eV for Sc) of the $2p^5$ shell and the e_g-t_{2g} crystal field splitting

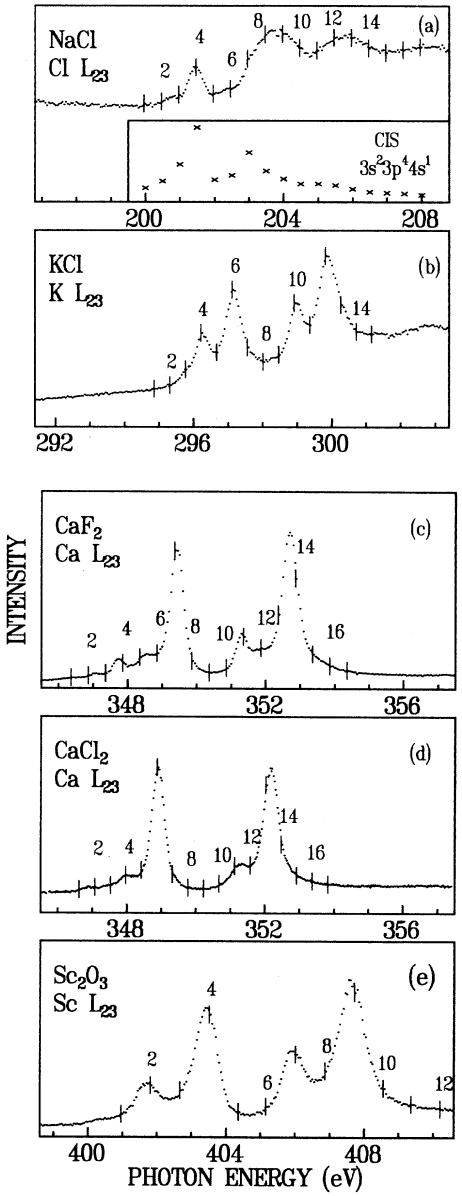

FIG. 1. L_{23} edges for NaCl (a), KCl (b), CaF_2 (c), $CaCl_2$ (d), and Sc_2O_3 (e). The numbered vertical bars show the photon energies used to induce the electron spectra in Figs. 2–6. The inset in Fig. (a) shows the CIS spectrum for the Cl $3p^{-2}4s$ final state.

(by about 1 eV for KCl, 1.5 eV for $CaCl_2$ and CaF_2, and 2 eV for Sc_2O_3) of the $3d$ orbital. The widths of the bands have a significant phonon contribution.[9,19] In the compounds considered here the crystal field has opposite signs for K^+ and Ca^{2+} in CaF_2 and as a consequence the lowest-energy component of the $3d$ orbital has t_{2g} symmetry in the case of K^+ and e_g symmetry in the case of Ca^{2+}.

In the $2p^5(3s^2 3p^6)3d$ configuration of the Cl^- ion the $3d$ orbital is not collapsed[3] and the transitions to the d-like continuum start at photon energies around 205–210 eV.[20] It is generally accepted[21] that the near-edge structure of the Cl^- L_{23} absorption spectra just above 200 eV originates from the transitions $2p^6 \rightarrow 2p^5 4s$. The spin-orbit splitting of the $2p^5$ shell of Cl^- is about 1.6 eV.[17,20]

In Figs. 2–6 the photoemission spectra of NaCl, KCl, $CaCl_2$, CaF_2, and Sc_2O_3, induced by photons with different energies in the vicinity of the L_{23} absorption edges, are shown. For each compound the photoemission spectra were taken at fixed photon energy steps throughout the L_{23} edge (see Fig. 1) and subsequently normalized for photon flux. For CaF_2 and KCl the spectra are comparable to those obtained earlier.[22,23]

In general, all structures in these spectra, excluding the

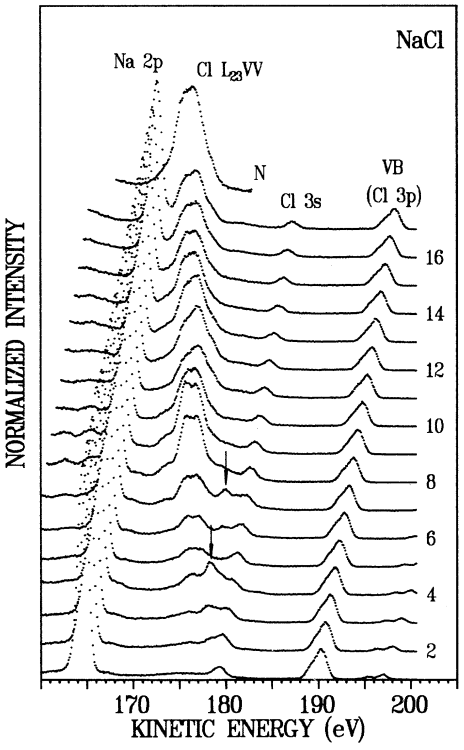

FIG. 2. Photoemission spectra for NaCl. The number at each spectrum corresponds to the vertical bar with the same number in Fig. 1 and shows the photon energy used. The spectra are normalized to equal photon flux. The energy levels and corresponding Auger transitions are indicated for most of the structures. The arrows indicate the spectator-induced structure in the Auger spectra. V stands for the valence band. N denotes the normal Auger spectrum excited by 220-eV photons.

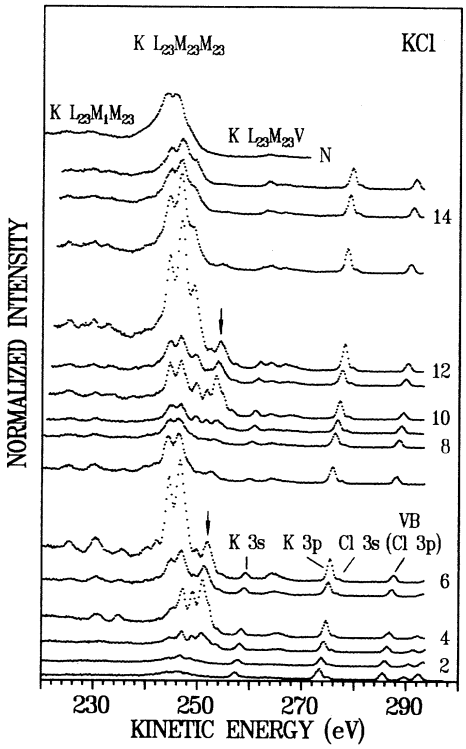

FIG. 3. The same as Fig. 2 for KCl. The normal Auger spectrum is excited by 400-eV photons.

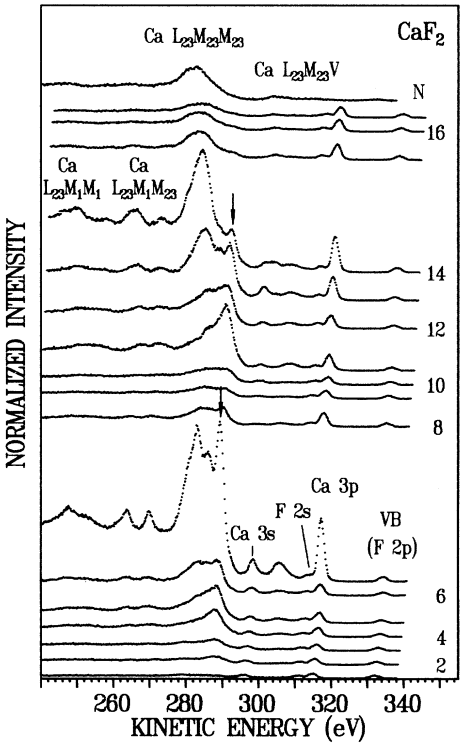

FIG. 4. The same as Fig. 2 for CaF_2. The normal Auger spectrum is excited by 400-eV photons.

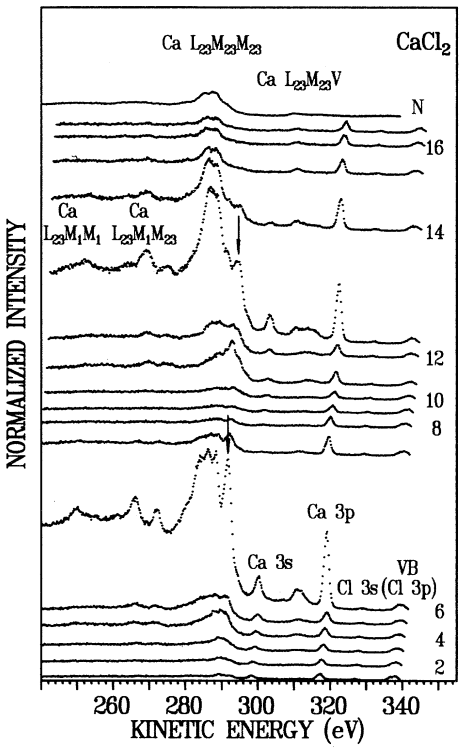

FIG. 5. The same as Fig. 2 for $CaCl_2$. The normal Auger spectrum is excited by 400-eV photons.

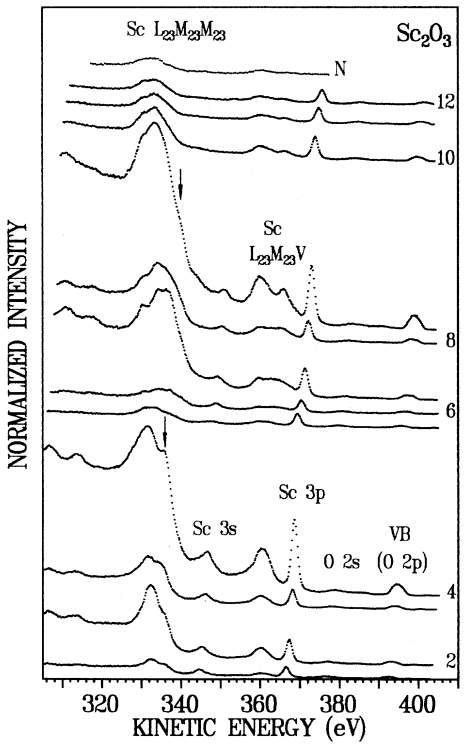

FIG. 6. The same as Fig. 2 for Sc_2O_3. The normal Auger spectrum is excited by 450-eV photons.

weak lines with energies exceeding the energies of valence electrons and which originate from the $2p$ electrons excited by second-order photons,[24] may be divided into two categories.

The first category consists of photoemission peaks originating from the photoionization of different energy levels of the crystal ions. The kinetic energies of these lines E_k vary linearly with photon energy $h\nu$ so that $E_k = h\nu - E_B$, E_B being the binding energy of the electron level. If the photon energy coincides with the $2p^6 \rightarrow 2p^5 3d$ absorption edge of K^+, Ca^{2+}, and Sc^{3+} the $3s$ and $3p$ photoemission peaks of these ions exhibit a resonant enhancement. This phenomenon is known as the participator effect of the excited ($3d$) electron and is due to its participation in the Auger decay channels $L_{23}M_{23}M_{45}$ and $L_{23}M_1M_{45}$ of the configuration $2p^5 3s^2 3p^6 3d$. At the resonant photon energies the final states created by either one of these Auger channels or by $3p$ and $3s$ direct photoionization become indistinguishable which leads to interference and in general a large enhancement of the $3p$ and $3s$ intensities in the electron

TABLE I. Experimental (E_B) and calculated (E_B^{th}) binding energies (in eV). E_B values are related to the maxima of the corresponding photoelectron lines referred to the bottom of the conduction band.

	NaCl		
Ion	Level	E_B	E_B^{th}
Cl	$3p$	10.2	9.2
Cl	$3s$	20.8	24.8
Na	$2p_{3/2}$		34.2
		35.3	
	$2p_{1/2}$		34.3
Cl	$2p_{3/2}$	203.1	203.0
	$2p_{1/2}$	204.7	204.6
	KCl		
Ion	Level	E_B	E_B^{th}
Cl	$3p$	9.6	8.7
Cl	$3s$	20.2	24.2
K	$3p_{3/2}$		20.6
		21.8	
	$3p_{1/2}$		20.8
K	$3s$	37.9	42.5
Cl	$2p_{3/2}$	202.9	202.5
	$2p_{1/2}$	204.5	204.1
K	$2p_{3/2}$	297.7	297.7
	$2p_{1/2}$	300.5	300.4
	CaF_2		
Ion	Level	E_B	E_B^{th}
F	$2p$	14.8	9.5
Ca	$3p_{3/2}$		28.2
		31.8	
	$3p_{1/2}$		28.5
F	$2s$	35.8	33.5
Ca	$3s$	50.7	53.2
Ca	$2p_{3/2}$	353.3	352.6
	$2p_{1/2}$	356.6	356.1

spectra.[25] The existence of such a participator enhancement is another indication of the $3d$ electron being localized in the parent ion, because such a localization is a necessity if participator Auger channels $L_{23}M_1M_{45}$ and $L_{23}M_{23}M_{45}$ are to have a significant intensity.

In Table I the experimental and computed values of E_B as explained in Sec. III are presented for NaCl, KCl, and CaF_2 crystals. The overall good agreement of the theoretical and experimental values testifies that a simple model correctly accounts for the polarization effects connected with the photoionization of atoms in ionic solids. The minor discord in the cases of the levels of s symmetry is due to strong collective effects in the ionization of these levels, not taken into account in our computational procedure.[26]

The second category of structures in Figs. 2–6 are the Auger electron peaks. All the spectra are dominated by strong $L_{23}M_{23}M_{23}$ Auger lines situated at 170–180 eV for Cl, 240–250 eV for K, 280–295 eV for Ca, and 325–340 eV for Sc. The weaker $L_{23}M_{23}V$ (V denotes the valence band), $L_{23}M_1M_{23}$ (for K and Ca) and $L_{23}M_1M_1$ (for Ca) Auger lines are also seen. The calculated normal Auger energies, shown in Table II excellently coincide with the measured ones for the $L_{23}M_{23}M_{23}$ case. In Fig. 7 we compare the full calculated K $L_{23}M_{23}M_{23}$ Auger spectrum of KCl with the spectral data. Note that no additional alignment of theoretical and experimental results has been performed. Except for a deviation in the relative intensities of the two most intense Auger bands the agreement is quite good.

The most striking effect seen in Figs. 2–6 is that small changes of the energy of the exciting photons in the regions of the $2p^6 \rightarrow 2p^5 3d$ resonance lead to drastic changes in the $L_{23}M_{23}M_{23}$ Auger spectra both in shape and intensity. Taking the normal Auger $L_{23}M_{23}M_{23}$ spectra as references these changes may be described as new structures appearing on the high-energy side. With increasing photon energy this so-called spectator structure shifts to higher energies.

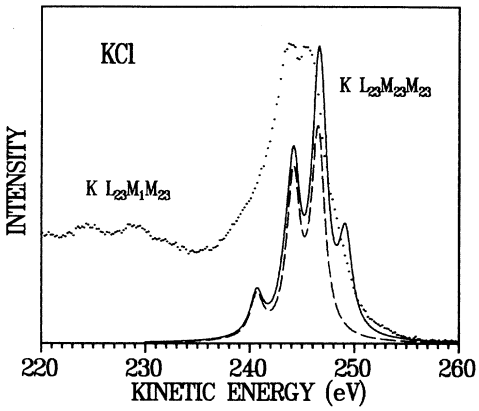

FIG. 7. The normal Auger spectrum for KCl, excited by 400-eV photons, and the calculated K^+ $L_{23}M_{23}M_{23}$ Auger spectrum (solid line), broadened with a Lorentzian of 1.5 eV FWHM. The dashed line shows the $L_3M_{23}M_{23}$ structure.

Generally speaking, these changes of the Auger spectra at the resonant excitation may be considered as a result of the spectator role of the excited $3d$ electron in the $L_{23}M_{23}M_{23}$ Auger transition in which it does not participate directly. Similar effects have been observed earlier for several atoms, molecules and solids (see, e.g., Ref. 1). They are due to screening by the excited (here $3d$) electron of the escaping Auger electron from the two-hole final state (here $3p^{-2}$). It turns out, however, that the spectator feature shifts with photon energy which is a comparatively novel finding. Something similar was found earlier for the $L_3M_4M_5$ ($^1G_4$) Auger spectrum of Xe atoms[27,28] and the $M_{23}M_{45}M_{45}$ Auger spectrum of solid Ge.[29] In general terms such an effect means that the Auger transition is so fast that at resonant photon ener-

TABLE II. Experimental (E_A) and calculated (E_A^{th}) Auger energies for the main LMM Auger transitions. Γ is the calculated partial width (in eV).

	Cl (NaCl)			K (KCl)			Ca (CaF_2)		
Assignment	E_A	E_A^{th}	Γ	E_A	E_A^{th}	Γ	E_A	E_A^{th}	Γ
$L_3M_{23}M_{23}(^1D_2)$		176.4		244	244.1			281.1	
$L_3M_{23}M_{23}(^3P_2)$	176	178.2	0.12		246.6	0.18	283	283.0	0.21
				246					
$L_2M_{23}M_{23}(^1D_2)$		178.0			246.9			284.6	
$L_3M_1M_{23}(^1P_1)$					217.6			251.1	
				224			258		
$L_2M_1M_{23}(^1P_1)$					220.4			254.6	
						0.049			0.055
$L_3M_1M_{23}(^3P_2)$					226.5			260.9	
				229			265		
$L_2M_1M_{23}(^3P_1)$					229.0			264.1	
$L_3M_1M_1(^1S_0)$					199.4			230.3	
						0.0013			0.0016
$L_2M_1M_1(^1S_0)$					202.1			233.8	

gies it is not possible to separate it from the photon absorption. Both processes together should then be considered as a single Auger resonant inelastic scattering event, a transition from the "ground-state ion (atom) + resonance photon" initial state to the "excited and ionized ion (atom) + escaping electron" final state.[2,28] The final-state ionic configuration has definite energy and long lifetime and is prepared faster than the "Auger" electron which leaves the ion carrying with it the excess photon energy. The atom remembers how it was excited and communicates this to us through the energy of the outgoing electron.

V. THE AUTOIONIZATION PROCESS

After the general points mentioned in the preceding section we will now deal with the peculiarities of each ion in a more detailed discussion of the resonant $L_{23}M_{23}M_{23}$ Auger spectra. We will compare the experimental results with theoretical calculations, and in order to follow the collapse of the $3d$ wave function we will deal successively with Cl^- in NaCl, K^+ in KCl, Ca^{2+} in CaF_2 and $CaCl_2$, and Sc^{3+} in Sc_2O_3. As will become clear, the comparison with theory proves to be particularly enlightening for K^+ in KCl. This subsection therefore carries our main discussion concerning the physical mechanism underlying the resonant Auger decay.

A. Cl^- in NaCl

In the case of Cl^- (Fig. 2) the spectator-induced structure appears at $h\nu \approx 201.5$ eV and peaks together with the first L_3 exciton absorption maximum. This is illustrated in more detail in Fig. 1(a), which in addition to the Cl L_{23} edge shows the normalized photoemission intensity of the spectator structure, or actually its constant initial-state (CIS) spectrum. The participator effect of the excited electron for the $3p$ and $3s$ photoelectron lines is very weak or absent. This is in line with the standpoint that the first maxima in the $Cl^- L_{23}$ absorption spectra of metal chlorides are due to the $2p^6 \rightarrow 2p^5 4s$ transitions, the final-state $4s$ electron being loosely bound to the parent Cl atom and having a mean radius comparable with the lattice parameter. The creation energy of the final configuration of the scattering event, the $3p^{-2}4s$ configuration, is about 23.2 eV. The appearance of the spectator-induced structure in the region of $h\nu \approx 203$ eV [see Fig. 1(a)] indicates that the $2p_{1/2}$ component of the L_{23} core exciton absorption is in the case of NaCl hidden in the wide absorption structure in the region of 203–204 eV, as proposed earlier.[20]

Although the $3d$ wave function is not collapsed in the case of the Cl^- $2p^5 3d$ configuration, an interesting weak high-energy feature seems to appear in the Cl^- $L_{23}M_{23}M_{23}$ Auger spectra at $204 < h\nu < 206$ eV (spectra 10–13 in Fig. 2). This feature may be interpreted as an nd-spectator-induced structure, which then means that the threshold energy for $2p^6 \rightarrow 2p^5 nd$ transitions for Cl^- in NaCl lies around 204 eV and that the $3d$ electron forms in the field of two $3p$ holes a short-living stationary state, degenerate with the s-type continuum.

B. K^+ in KCl

In order to understand the structures in the vicinity of the normal $L_{23}M_{23}M_{23}$ Auger structure of KCl (Fig. 3) in some more detail we show in Fig. 8 as function of photon energy the energy position of the two highest-energy bands of the spectator structure as well as of a peak (coinciding with the maximum of spectrum 6), which is part of a structure nearly degenerate with the normal Auger one, and which starts to be clearly observable in spectrum 5, i.e., at $h\nu \approx 296.5$ eV. The almost linear dispersion of the first two structures throughout the whole resonance region, as is clear from comparison with the dispersion of the $3s$ photoemission line in Fig. 8, indicates that the final state arising from different resonances is always the same, i.e., it does not depend on the intermediate state. The lower-energy structure, on the other hand, essentially seems to remain at constant kinetic energy. Toward higher-photon energy (spectra 14 and 15) it can be seen that this peak finally merges with the ^3P peak of the normal $L_3M_{23}M_{23}$ Auger structure. The deviation of the dispersion from a strict linearity in the regions of the first and third absorption peaks seems systematic and could be due to an energy redistribution between escaping electrons and phonons, or to an interference (Fano) effect.

Since the final configuration for the normal $L_{23}M_{23}M_{23}$ Auger transition in K^+ is $1s^2 2s^2 2p^6 3s^2 3p^4$ (or $3p^{-2}$), the final configuration for the same transition in the presence of a $3d$ spectator electron should be $3p^{-2}3d$. This configuration has been shown to be the main product of the resonant Auger transitions in Ar atoms[30,31] and it is also observable among the products of similar transitions in K and Ca atoms.[32,33] The creation energies corresponding to the main maxima of the spectator-induced Auger structure, 45.6, 47.5, 49.5, and 51.5 eV, are in the same energy region as the energies of various terms of the $3p^{-2}3d$ configuration of K^+ free ions.[34]

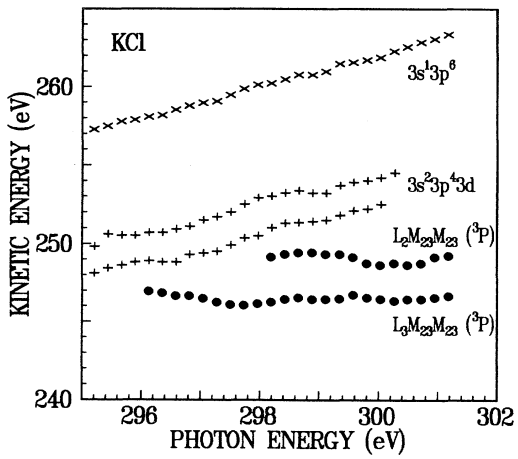

FIG. 8. The energy position of the K $3s$ photoemission line of KCl (×), the two high-energy spectator satellites (+), and the ^3P peaks of the $L_{23}M_{23}M_{23}$ Auger structure (dots) as function of photon energy.

To separate the dispersive and nondispersive structures we shift spectrum 4 with respect to spectrum 6 by the difference in photon energy and renormalize its intensity so that the highest-energy spectator lines in the spectra 4 and 6 coincide. The difference of the spectra 6 and 4 obtained after this procedure is shown in Fig. 9(b). The comparison of the difference spectrum with the calculated $L_3M_{23}M_{23}$ Auger structure, also presented in Fig. 9(b), suggests that it can indeed be ascribed to a normal $L_3M_{23}M_{23}$ Auger structure presumably shifted to higher energies by about 1 eV, as can be seen by comparing spectrum 15 and the normal Auger spectrum in Fig. 3. At the position of ^1S term of the Auger structure some additional weak features are seen, for which, however, we have no explanation. Similarly, we conclude that spectrum 12 in addition to the spectator structure and a normal $L_3M_{23}M_{23}$ Auger structure contains the normal $L_2M_{23}M_{23}$ Auger structure. The comparison of spectra 10–12 with each other shows that the latter starts to arise in spectrum 11, i.e., at $h\nu \approx 299.3$ eV. The energy position of the identified ^3P line of this $L_2M_{23}M_{23}$ structure again proves to be essentially nondispersive, as shown in Fig. 8.

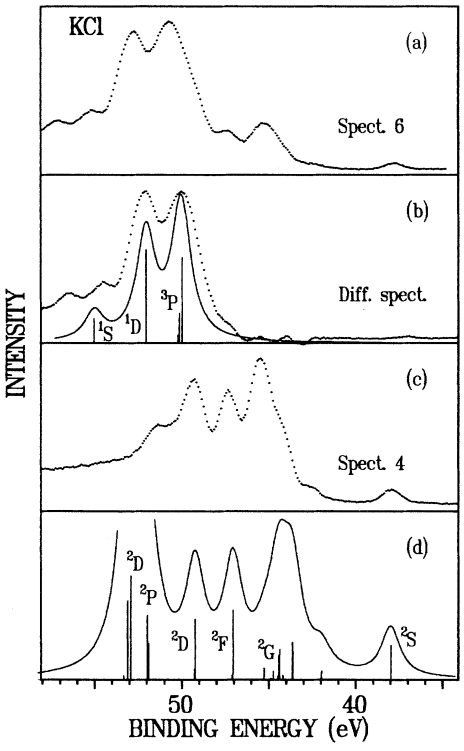

FIG. 9. Resonant $L_{23}M_{23}M_{23}$ Auger spectra for KCl as compared to the calculation of the $3s^2 3p^4 3d$ and $3s 3p^6$ final states. In (a) and (c) are shown spectra 6 and 4 of Fig. 3, respectively. Their difference spectrum is shown in (b) and compared with the calculated $L_3M_{23}M_{23}$ Auger structure (solid line). Our calculation of the $3p^{-2}3d^1$ configuration of the $L_2M_{23}M_{23}$ autoionization spectrum is shown in (d). The theoretical multiplets are broadened with a Lorentzian of 1.5 eV FWHM. Further explanation in text.

This decomposition procedure leads to the conclusion that at resonant $2p^6 \rightarrow 2p^5 3d$ excitation the photoemission spectra of K^+ in the vicinity of the $L_{23}M_{23}M_{23}$ Auger structure contains three components, the spectator-induced structure, which shifts to higher-kinetic energy with increasing photon energy, and the normal $L_3M_{23}M_{23}$ and $L_2M_{23}M_{23}$ Auger structures. The small high-energy shift of this Auger structure at photon energies close to the ionization threshold may be understood as the PCI of the slow photoelectron and the fast Auger electron.[2]

Although in a straightforward treatment the development of the $3p^{-2}3d$ final configuration at resonant photon energies should be considered as the result of a single scattering event $2p^6 + h\nu \rightarrow 3p^{-2}3d + e$, we treat it here as a two-step process, the first step being the creation of the $2p^{-1}3d$ excited configuration and the second one the spectator decay $2p^{-1}3d \rightarrow 3p^{-2}3d + e$ of this configuration. On these grounds we use the model explained in Sec. III to compute the spectator structure in the electron spectra as the structure which corresponds to this second step. In Fig. 9(a) this result is shown. The $^3D_1$ state was chosen as the atomic intermediate state. For this state the probability of a $2p_{3/2}$ hole is largest. It should, however, be noted that the Auger intensity distribution does not critically depend on the choice of the intermediate state. Note, also, that for this more detailed comparison we have aligned and compressed the energy scale of the calculated spectrum. The compression (here 85%) is a common practice to correct for the configuration interaction and the solid state effects not considered in our calculations. This many-body correction can, for instance, also be achieved by a renormalization of the Slater integrals involved.[35] Either method yields in essence the same result.

After this correction we find for the spectrum in Fig. 9(c) a good agreement in position and relative intensity of the indicated $(^1D)3d^2D$, $(^1D)3d^2F$ terms and the ^2S term, which coincides with the $3s$ photoemission line. The $3p^4$ parent terms are given in parentheses. Note that the intensity of the $3s$ photoemission line is determined by interference effects with the direct photoemission process. This effect is neglected in a two-step approach. The position of the most intense spectator peak differs by about 1.5 eV from the theoretical result, but this discrepancy can be understood from the multitude of terms (15 in total) which contribute to its intensity. The relative balance of the Auger intensities is in a rather subtle way dependent on the final-state potential, which determines the shape of the continuum wave function and the value of the radial integrals. The Auger intensities are therefore easily affected by the approximations in our scheme, and we believe that the cause of the discrepancy here is the intensity of the ^2G term which seems strongly underestimated in the calculation. There is, however, a much stronger discrepancy between calculation and experimental result, because intensity in the $(^1D)3d^2D$ and $(^1D)3d^2P$ terms at higher-binding energy seems completely lacking. We suggest, that this is caused by the fact that at these energies the $3p^4 3d$ multiplet states are degenerate with the final state of the $3p^4$ normal Auger

processes. The underlying physics is that the excited $3d$ electron in the intermediate $2p^5 3d$ state has a certain probability to be delocalized. This probability depends on the particular resonance, or more specifically on the wave function of the $3d$ electron in the crystal field and the coupling of the $3d$ state with the conduction band continuum. This should also affect the fate of the $3d$ wave function in the final two-hole configuration, where it may or may not collapse progressively to form the $3p^4 3d^1$ multiplet state. In Fig. 9(b) it can be seen that the ^1D term of the experimentally determined $L_3M_{23}M_{23}$ structure, which is the parent structure of the lacking spectator terms, can be considered to mark the energy boundary between both possible decay processes.

For higher-photon energies exactly the same process takes place in relation to the $2p_{1/2}^{-1}3d$ configuration and the observed $L_2M_{23}M_{23}$ structure (starting at spectrum 10). But here also a relatively strong $L_3M_{23}M_{23}$ structure is observed. The latter is a consequence of the generally very fast $L_2L_3M_{45}$ Coster-Kronig (CK) process involving the $3d$ electron, which escapes into the continuum leaving the $2p_{3/2}^{-1}$ configuration. The additional Lorentzian broadening found in the "L_2" part of the absorption spectrum is a signature of this additional decay channel.[9]

It is important to note that the same final configuration $3p^{-2}3d$ arises as the cause of satellite structures in the L_{23} emission spectra of K^+ in potassium halides (the $2p^5 3s^2 3p^6 \rightarrow 2p^6 3s^2 3p^4 3d$ satellites of the $2p^5 3s^2 3p^6 \rightarrow 2p^6 3s^1 3p^6$ diagram lines[36,37]) and in the $3s$ photoelectron spectra.[38] The spectator as well as participator structures can therefore actually be considered as photoemission structures that resonate at the $2p$ core level threshold. The energy of the center of gravity of the satellite emission band is about 249 eV for KCl,[36] in excellent agreement with the energy of the center of gravity of the spectator structure in spectrum 4 (Figs. 3 and 9).

In Fig. 10 the excitation spectra for the highest-energy spectator structure, the $L_3M_{23}M_{23}(^3P)$ normal Auger structure as well as for the $3p$ and $3s$ photoemission lines are shown. They are essentially the CIS spectra for the photoelectron lines and the spectator structure and the constant final-state (CFS) spectra for the Auger line. It is clearly seen that the efficiencies to excite the spectator structure on the one hand and the Auger structure on the other compete with each other. The efficiency to excite the spectator structure is the largest in the regions of the first and third resonances, the efficiency to excite the Auger structure is the largest in the regions of the second and fourth resonances. Such a behavior of the excitation spectra can be considered as evidence for the fact that the high-energy components of the crystal-field-split $3d$ state reflected by the second and fourth resonances overlap the conduction band continuum and that the $3d$ electron excited to these states is partly delocalized, i.e., has a finite probability of leaving the region of the ion before the Auger transition occurs. The spectator structure is especially heavily suppressed in the high-energy region of the fourth resonance where it overlaps with the L_2 continuum, and where, as noted before, in addition part of the L_2 holes are transferred into L_3 holes via a CK transition before the Auger transition occurs.

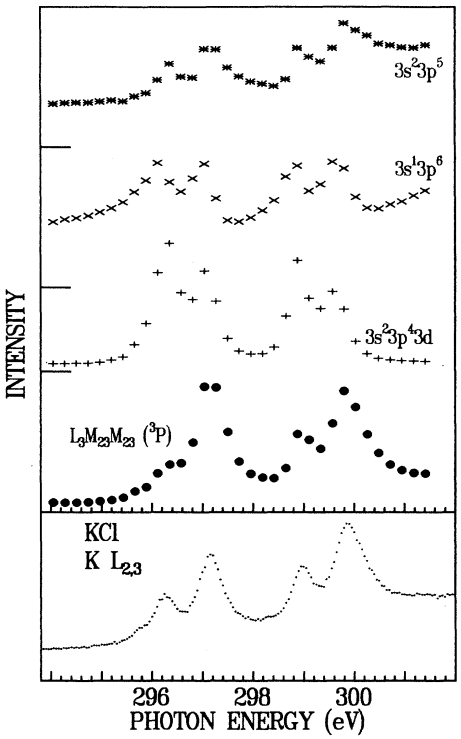

FIG. 10. The (CIS or CFS) excitation spectra for the $3p$ (*) and $3s$ (×) photoemission lines of KCl, as well as for the high-energy spectator structure (+) and the ^3P $L_3M_{23}M_{23}$ Auger line (dots), as compared with the K L_{23} edge. The excitation spectra are normalized for equal peak height; zeros are indicated by horizontal bars.

The efficiency of the participator role of the $3d$ electron (see Fig. 10) peaks at all four resonances, but the relative efficiency of the $3s$ photoelectron line is suppressed in the regions of the second and fourth resonances and seems to follow the efficiency of the spectator structure. This may be considered as an indication of the strong configuration interaction between the $3s3p^6$ and $3s^2 3p^4 3d$ configurations. It may also explain why the resonance maxima of the $3s$ and $3p$ photoemission lines do not coincide. Note that for the detailed discussion of the fate of the excited $3d$ electron the $3s \rightarrow 2p$ and $3d \rightarrow 2p$ radiative decay channels, not studied here, should be included.

The spectator effect manifests also itself in the $L_{23}M_1M_{23}$ and $L_{23}M_{23}V$ Auger spectra. It is observable in spectra 3–5 in Fig. 3 that both of these structures seem to have components shifted to higher energy in comparison with corresponding structures in, for example, spectra 7 and 8 or above the edge. Spectrum 6 demonstrates how the spectator-induced structures reduce to the normal spectra. In the region of the L_2 resonance (spectra 10–12) these spectator-induced structures appear again. It is, however, difficult from our data to say anything more definite about their dispersion.

To conclude, the resonant photoemission spectra of KCl at the L_{23} edge in the vicinity of the K $L_{23}M_{23}M_{23}$

Auger structure can be explained, accepting three statements.

(i) These spectra contain two major competing components, the PCI-shifted normal $L_3M_{23}M_{23}$ and $L_2M_{23}M_{23}$ structures and the spectator structure which shifts to higher energies almost linearly with increasing photon energy. The normal Auger structures are a signature of the delocalization of the $3d$ electron. As such, the presence of these structures may be considered as a solid-state effect.

(ii) The spectator structure is due to the $3p^{-2}3d$ final configuration and is always the same independently of the nature of the primary resonance; in its most pure form it can be observed only in the region of the first L_3 resonance, where its essentially atomic origin can be verified.

(iii) At the "L_2" part of the L_{23} edge, where the probability of creating $2p_{1/2}$ holes is largest, an additional $L_2L_3M_{45}$ CK process carries a large part of the weight of the deexcitation. The presence of an intense $L_3M_{23}M_{23}$ structure is assumed to be a proof of this.

C. Ca^{2+} in CaF_2 and $CaCl_2$

From a general point of view the situation with the $L_{23}M_{23}M_{23}$ Auger spectra and their $3d$-spectator-induced changes in the case of Ca^{2+} in CaF_2 and $CaCl_2$ (Figs. 4 and 5) should be similar to the situation for K^+ in KCl. Here also a spectator-induced structure appears for resonant photon energies at the high-energy side of the normal Auger structure and moves to higher energies as $h\nu$ increases. The creation energy of the highest-energy component of this final state configuration is about 57.3 eV. Also here we may conclude that the spectator structure is due to the final configuration $3p^{-2}3d$.

However, a more detailed analysis shows that the case of Ca^{2+} differs from the case of K^+ in some important aspects. Figure 11 illustrates some of the differences involved. We have compared similar spectra as in the case of KCl, with the atomic calculation here for CaF_2 and $CaCl_2$. The energy scale of the calculation was again compressed by 85%. We observe, first, that although the spectator peak at low-binding energy reasonably aligns with the theoretical result, there are, for both CaF_2 and $CaCl_2$, no further obvious agreements between spectral data and theory. Second, although components of the normal $L_3M_{23}M_{23}$ Auger structure may be present, they seem to be much weaker and also cannot be demonstrated by means of a subtracting technique as in the case of KCl, because of the intrinsic differences in these spectra. It may then, for example, be that all resonantly excited structure is spectator structure and that this structure depends on the nature of the primary photoexcitation resonance. Spectrum 11 in Fig. 4 (CaF_2) is very similar to spectra 4 and 5 showing that the replacement of the $2p_{3/2}$ hole by the $2p_{1/2}$ hole does not change the decay process of this resonance, except for the possible inclusion of an effective $L_2L_3M_{45}$ CK-like transition in the latter case. In the region of the highest-energy $2p_{1/2}^{-1}3d$ resonance (spectra 12–14 in Fig. 4 as well as in Fig. 5) the situation

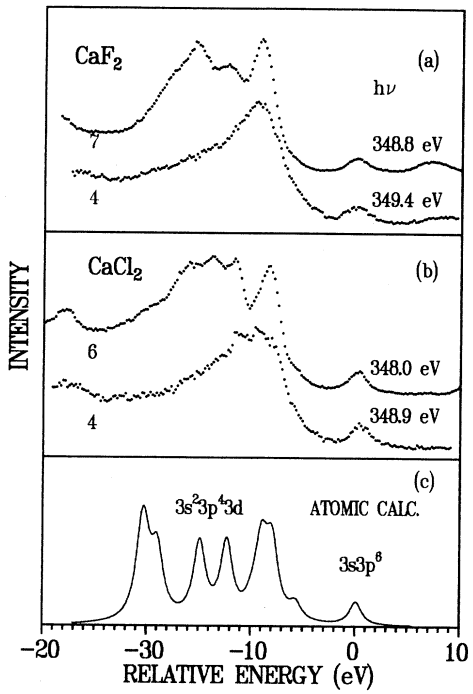

FIG. 11. (a) Resonant $L_{23}M_{23}M_{23}$ Auger spectra for CaF_2 (spectra 4 and 7 of Fig. 4). (b) Resonant $L_{23}M_{23}M_{23}$ Auger spectra for $CaCl_2$ (spectra 4 and 6 of Fig. 5). (c) The atomic calculation for the $3s^23p^43d$ and $3s3p^6$ final states, broadened with a Lorentzian of 1.5 eV FWHM.

differs to the extent that the spectator decay is suppressed and that a very strong $L_2L_3M_{45}$ CK transition, indicated by a large $L_3M_{23}M_{23}$ normal Auger structure, dominates. Note that the participator-induced enhancement of the $3s$ and $3p$ photoelectron lines is relatively strong as compared to the case of K^+.

Looking for a physical difference between the cases of K^+ and Ca^{2+} it should be noted that the $2p^53d$ configuration in Ca^{2+} is more localized because of the progressed collapse of the $3d$ wave function, and that its binding energy is larger. This may explain the lack of a clear normal Auger component (except for the one caused by the CK process) in the deexcitation spectra. In the case of KCl the crystal field did not seem to prevent a comparison with the atomic calculation. But, the intrinsic differences in the autoionization spectra of CaF_2 and $CaCl_2$ may be indicative of a crystal-field effect that cannot be neglected.

D. Sc^3 in Sc_2O_3

The resonantly excited electron spectra of Sc^{3+} in Sc_2O_3 in the $L_{213}M_{23}M_{23}$ Auger region are considerably wider and less structured than those of K^+ and Ca^{2+}. The probable cause for this is that the chemical bond in Sc_2O_3 is much more covalent than in KCl, CaF_2, or $CaCl_2$. An important consequence of this circumstance is that all the $2p^53d$ resonant absorption structure is degenerate with the conduction band continuum. This may ex-

plain why in Fig. 6 structures identifiable with the normal $L_3M_{23}M_{23}$ as well as the $L_3M_{23}V$ Auger structures appear already at the first $2p^53d$ resonance. Further evidence of this covalency effect, which follows also from a detailed analysis of the L_{23} edge,[9] is presented by the resonant enhancement of the valence band, clearly observable in spectra 4 and 9 of Fig. 6. This can only be caused by the presence of Sc d character in the occupied part of the valence band. Nevertheless, the traces of what we should identify as a spectator structure shifting to higher energies with increasing photon energy are seen in some of the spectra. The creation energy corresponding to this final-state structure is about 68 eV. As in the cases of K^+ and Ca^{2+} we assume a $3p^{-2}3d$ intermediate configuration to be responsible for this structure. Part of the normal $L_3M_{23}M_{23}$ structure at the "L_2" resonance should, finally, be attributed to a CK-mediated decay process.[9]

VI. SHAKE PROBABILITIES

If our interpretation of the spectator-induced spectra is correct, there remains no apparent structure to be interpreted involving a shake-off or shake-up of the excited $3d$ or $4s$ electron during the Auger decay of the $2p$ hole. This is in contrast to the case of Ar atoms where the shake-up processes (mainly $3d\rightarrow 4d$ and $4s\rightarrow 5s$) were shown to play an important role in the formation of the final state.[30,31] To solve this contradiction we have calculated the total overlap probabilities P_{nl} to verify that no ejection or excitation of $3d$ and $4s$ electrons of the configurations $2p^53s^23p^63d(4s)$ takes place during the $L_{23}M_{23}M_{23}$-like deexcitation (Table III). This overlap is given approximately by the formula

$$P_{nl}=\left[\int R^i_{nl}R^f_{nl}r^2dr\right]^2, \tag{6}$$

where R^i_{nl} and R^f_{nl} are the initial and final state radial wave functions of nl ($3d$ or $4s$) electrons, respectively. As seen in Table III, for $3d$ electrons $\langle r_{nl}\rangle$ decreases sharply in the sequence from Ar to Ca^{2+}. In the case of Ar the $3d$ electron collapses during the Auger decay and the shape probability is large, while for K^+ and even more for Ca^{2+} it is completely collapsed in the $2p^53d$ configuration. During the Auger decay its mean radius changes little and the shake probability is small. Another factor which decreases the shake-up probability for the $3d$ electron is the fact that, in the configuration $2p^5nd$ ($n\geq 4$) of ions considered here, the d electron is not collapsed and contributes to the crystalline states which have low density at any particular ion state. Therefore, we cannot support the suggestion of Ref. 22 that the shake processes are important to the build up of the $3d$ spectator structure in the case of Ca^{2+} in CaF_2.

VII. CONCLUSIONS

We have demonstrated that at incident photon energies coinciding with the $2p^6\rightarrow 2p^53d(4s)$ resonances in the absorption spectra of argonlike ions Cl^- (in NaCl), K^+ (in KCl), Ca^{2+} (in $CaCl_2$ and CaF_2), and Sc^{3+} (in Sc_2O_3) the spectra of electrons emitted by these ions contain a spectator structure in the region of the $L_{23}M_{23}M_{23}$ normal Auger structures and that this structure shifts to higher kinetic energies with increasing photon energy. Both empirical considerations and Hartree-Fock-Pauli computations show that this structure originates from the $3p^{-2}3d(4s)$ final configuration arising as a product of the Auger resonant inelastic scattering process of incident photons. Collapse of the $3d$ electron in the $2p^53d$ configuration in the sequence $Cl^-\rightarrow Ar\rightarrow K^+$ leads to the marked increase of intensity of this process and the decrease of the role of shake processes in it. Our experimental data for Cl^- in NaCl and K^+ in KCl are clear evidence of this.

One of the main points of this study is that we propose that also the spectator structures, to the extent they are present in the resonant $L_{23}M_{23}M_{23}$ Auger structures, essentially remain at constant binding energy. Our reason for this assumption is that we consider both participator and spectator processes as decay channels to a single photoemission final state, the "main" photoemission line and its configuration interaction (CI) satellites. At resonance the intensity ratio of main line and CI satellites may, of course, completely change, because of the in-

TABLE III. The calculated probabilities P_{nl} for $3d$ and $4s$ electrons not to be ejected or excited during the Auger decay. $\langle r_{nl}\rangle$ is the mean radius of the nl excited electron wave function (in atomic units).

Initial and final configurations		Cl (NaCl)		Ar		K (KCl)		Ca (CaF_2)	
		$\langle r_{nl}\rangle$	P_{nl}	$\langle r_{nl}\rangle$	P_{nl}	$\langle n_{nl}\rangle$	P_{nl}	$\langle r_{nl}\rangle$	P_{nl}
Initial	$2p^53s^23p^63d$			9.24		2.92		1.63	
					0.23		0.86		0.99
Final	$2p^63s^23p^43d$			2.79		1.85		1.47	
Initial	$2p^53s^23p^63d$			9.24		2.92		1.63	
					0.17		0.82		0.98
Final	$2p^63s^03p^63d$			2.46		1.75		1.43	
Initial	$2p^53s^23p^64s$	5.67		5.34					
			0.88		0.87				
Final	$2p^63s^23p^44s$	4.43		4.10					

volvement of different matrix elements and selection rules. The dispersion curves of Fig. 8 could with regard to spectator structures, in principle, also be interpreted as pointing to a stepwise increase in kinetic energy, corresponding to the four (more or less relaxed) intermediate states. A fitting procedure was used to compose this figure and the data do not seem to exclude such a mechanism. However, we would want to argue in favor of the first mechanism, i.e., an altogether coherent process, because of its physical clarity and its theoretical attractiveness within the scheme of a single-step model.

In the case of Cl^- the lower resonances are due to the $2p^{-1}4s$ configuration which results in a $3p^{-2}4s$ final configuration. In the case of the metal ions, our spectra demonstrate the occurrence of a $L_2L_3M_{45}$ Coster-Kronig process which can be considered as evidence for the localization (collapse) of the $3d$ wave function. But, in spite of a general similarity, the details of the spectra of the metal ions studied here differ from each other. The main reason is the different coupling to the $2p^5 3d$ bound states with the conduction band continuum. In the case of Sc^{3+} all the intermediate states lie in the continuum, and the excited $3d$ electron is substantially delocalized and the spectra are dominated by $L_3M_{23}M_{23}$ and $L_2M_{23}M_{23}$ Auger structures. In the case of K^+ only the lowest-order resonance seems completely localized and gives rise to a pure spectator structure which has an atomic origin as verified by our calculations. For Ca^{2+} the intermediate states seem nearly completely localized and give rise to a complicated "spectator" structure, indicating a possible additional role of the crystal field. However, to reach a full understanding of the latter a more detailed theoretical analysis with inclusion of crystal field effects may prove to be of importance.

ACKNOWLEDGMENTS

This work was supported by the Swedish Natural Sciences Research Council, the Crafoord Foundation, and the Royal Swedish Academy of Sciences. We wish to acknowledge stimulating discussions with Professor T. Åberg, Professor S. Aksela, Dr. J. Tulkki, Dr. H. Aksela, and Dr. A. Maiste. We thank A. Kasikov for providing the samples of Sc_2O_3.

[1]Several papers on this topic have recently appeared in the *Proceedings of the 2nd International Workshop on Auger Spectroscopy and Electron Structure* (IWASES-II), Malmö, Sweden, 1991, edited by K. Wandelt, C.-O. Almbladh, and R. Nyholm [Phys. Scr. **T41** (1992)].

[2]T. Åberg, Phys. Scr. **T41**, 71 (1992).

[3]A. A. Maiste, R. E. Ruus, and M. A. Elango, Zh. Eksp. Teor. Fiz. **79**, 1671 (1980) [Sov. Phys. JETP **52**, 844 (1980)].

[4]J. N. Andersen, O. Björneholm, A. Sandell, R. Nyholm, J. Forsell, L. Thånell, A. Nilsson, and N. Mårtensson, Synchrotron Radiat. News **4**, 15 (1991).

[5]R. T. Poole, J. G. Jenkin, J. Liesegang, and R. C. G. Leckey, Phys. Rev. B **11**, 5179 (1975).

[6]S. Muramatsu and C. Sugiura, Phys. Rev. B **27**, 3806 (1983).

[7]G. W. Rubloff, Phys. Rev. B **5**, 662 (1972).

[8]H. H. Tippins, J. Phys. Chem. Solids **27**, 1069 (1966).

[9]F. M. F. de Groot, J. C. Fuggle, B. T. Thole, and G. A. Sawatzky, Phys. Rev. B **41**, 928 (1990).

[10]P. H. Citrin, P. Eisenberger, and D. R. Hamann, Phys. Rev. Lett. **33**, 965 (1974).

[11]R. Karazija, *The Theory of X-Ray and Electronic Spectra of Free Atoms. An Introduction* (Mokslas, Vilnius, 1987, in Russian); E. J. McGuire, in *Atomic Inner-Shell Processes: I. Ionization and Transition Probabilities,* edited by B. Crasemann (Academic, New York, 1975), pp. 293–330.

[12]Z. B. Rudzikas, in *Proceedings of the 6th International Conference on Atomic Physics,* Riga, USSR, edited by R. Damburg, (Zinatne, Riga; Plenum, New York and London, 1979), pp. 92–110.

[13]R. E. Watson, Phys. Rev. **111**, 1108 (1958).

[14]T. Chassé, R. Franke, P. Struebel, and A. Meisel, Phys. Scr. T **41**, 281 (1992).

[15]G. D. Mahan, Phys. Rev. B **22**, 3102 (1980).

[16]R. T. Poole, J. Szajman, R. C. G. Leckey, J. G. Jenkin, and J. Liesegang, Phys. Rev. B **12**, 5872 (1975).

[17]Y. Iguchi, T. Sagawa, S. Sato, M. Watanabe, H. Yamashita, A. Ejiri, M. Sasanuma, S. Nakai, M. Nakamura, S. Yamaguchi, Y. Nakai, and T. Oshio, Solid State Commun. **6**, 575 (1968).

[18]R. E. Ruus, Opt. Spectrosc. **59**, 450 (1985).

[19]F. Sette, B. Sinkovic, Y. J. Ma, and C. T. Chen, Phys. Rev. B **39**, 11 125 (1989).

[20]A. M.-E. Saar and M. A. Elango, Fiz. Tverd. Tela (Leningrad) **13**, 3532 (1971) [Sov. Phys. Solid State **13**, 2985 (1971)].

[21]See, for example, O. Björneholm, A. Sandell, A. Nilsson, N. Mårtensson, and J. N. Andersen, Phys. Scr. T **41**, 217 (1992).

[22]T. Tiedje, K. M. Colbow, D. Rodgers, and W. Eberhardt, Phys. Rev. Lett. **65**, 1243 (1990).

[23]A. Kikas, A. Ausmees, M. Elango, J. N. Andersen, R. Nyholm, and I. Martinson, Europhys. Lett. **15**, 683 (1991).

[24]These lines provide a further check of the energy position of the absorption threshold relative to the $2p$ binding energy.

[25]U. Fano, Phys. Rev. **124**, 1866 (1961).

[26]M. Ohno, J. Electron Spectrosc. Relat. Phenom. **48**, 125 (1989).

[27]G. S. Brown, M. H. Chen, B. Crasemann, and G. E. Ice, Phys. Rev. Lett. **45**, 1937 (1980).

[28]G. B. Armen, T. Åberg, J. C. Levin, B. Crasemann, M. H. Chen, G. E. Ice, and G. S. Brown, Phys. Rev. Lett. **54**, 1142 (1985).

[29]A. Kivimäki, H. Aksela, S. Aksela, and O.-P. Sairanen, Phys. Rev. B (to be published).

[30]H. Aksela, S. Aksela, H. Pulkkinen, G. M. Bancroft, and K. H. Tan, Phys. Rev. A **37**, 1798 (1988).

[31]M. Meyer, E. v. Raven, B. Sonntag, and J. E. Hansen, Phys. Rev. A **43**, 177 (1991).

[32]M. Meyer, E. v. Raven, M. Richter, B. Sonntag, and J. E. Hansen, J. Electron Spectrosc. Relat. Phen. **51**, 407 (1990).

[33]M. Meyer, E. v. Raven, M. Richter, B. Sonntag, R. D. Cowan, and J. E. Hansen, Phys. Rev. A **39**, 4319 (1989).

[34]C. E. Moore, *Atomic Energy Levels as Derived from the Analysis of Optical Spectra,* National Bureau of Standards Circular No. 467 (U.S.G.P.O., Washington, D.C., 1949).
[35]R. D. Cowan, *The Theory of Atomic Structures and Spectra* (University of California Press, Berkeley, 1981).
[36]B. Sorkin, A. Saar, and M. Elango, Toim, Eesti NSV Tead. Akad. Fuus. Mat. (USSR) **22**, 105 (1973).
[37]J. Valjakka, J. Phys. C **19**, 1451 (1986).
[38]G. K. Wertheim and A. Rosencwaig, Phys. Rev. Lett. **26**, 1179 (1971).